Electronic spectrum of jet cooled SiCN

Masaru Fukushima and Takashi Ishiwata

Citation: The Journal of Chemical Physics **145**, 124304 (2016); doi: 10.1063/1.4962504
View online: http://dx.doi.org/10.1063/1.4962504
View Table of Contents: http://aip.scitation.org/toc/jcp/145/12
Published by the American Institute of Physics

Electronic spectrum of jet cooled SiCN

Masaru Fukushima[a] and Takashi Ishiwata
Faculty of Information Sciences, Hiroshima City University, Hiroshima 731-3194, Japan

(Received 3 July 2016; accepted 29 August 2016; published online 23 September 2016)

We have generated SiCN in a supersonic free expansion, and measured the laser induced fluorescence (LIF) spectrum. Prior to the experiments, *ab initio* calculations were carried out to obtain the information necessary for searching for the LIF signals. In addition to the $\tilde{X}\ ^2\Pi$ state, the optimized structures of three excited states, $^2\Delta$, $^2\Sigma^+$, and $^2\Sigma^-$, have been obtained. Guided by the predictions, the LIF excitation spectrum of SiCN was observed in the UV region. The rotational structure of the 0_0^0 band with the origin, 29 261.639 cm^{-1}, indicated that the electronic transition is $\tilde{A}\ ^2\Delta$–$\tilde{X}\ ^2\Pi$. The spin-orbit (SO) constants of the $\tilde{X}\ ^2\Pi$ and $\tilde{A}\ ^2\Delta$ states were determined to be 140.824 and 4.944 cm^{-1}, respectively. In the $\tilde{A}\ ^2\Delta$ state, the Fermi resonance between the $(0,2^0,0)\ ^2\Delta$ and $(0,0^0,1)\ ^2\Delta$ vibronic levels was identified. The molecular constants of the $\tilde{X}\ ^2\Pi$ state were determined through the simultaneous analysis of the combination differences derived from the present LIF data with the previously reported rotational transitions. The spectroscopic parameters of the $\tilde{A}\ ^2\Delta$ state were also obtained from the analysis where the constants of the $\tilde{X}\ ^2\Pi$ state, derived above, were fixed at those values. *Published by AIP Publishing.* [http://dx.doi.org/10.1063/1.4962504]

I. INTRODUCTION

Silicon-bearing species existing under extreme environments, such as high temperature and discharge plasma conditions, have attracted much attention in a wide range of fields. One of the fields is material manufacturing processes. Under plasma chemical vapor deposition (CVD) processes to grow *a*-Si films, it was reported that some silicon containing species have important roles for the characteristics of the films produced.[1] Another field is astronomical observations. Because of the substantial cosmic abundance of Si, several silicon containing species have been detected in circumstellar envelopes; such as SiC, SiN, SiO, SiS, *c*-SiC_2, SiCN, *c*-SiC_3, and SiC_4.[2]

SiCN and SiNC were first observed as the reaction intermediates from the reaction of silicon atom with hydrogen cyanide, HCN, in an Ar matrix, and the vibrational spectra were assigned on the basis of *ab initio* calculations.[3] In the gas phase, these species were first observed by rotational spectroscopy. They were observed as the discharge products of silane and cyanoacetylene in supersonic free jet expansions by the Fourier transform microwave spectroscopy, and also as those products from a silane, nitrogen, and acetylene mixture in a flow cell by millimeter-wave spectroscopy.[4,5] This laboratory detection was benefited by calculational work.[6,7] Following the precise molecular constants obtained from laboratories, the astronomical detection of SiCN was subsequently reported in the carbon star IRC+10216.[8] The isomerization process between these species, SiCN ⇌ SiNC, in the ground $^2\Pi$ state was studied by *ab initio* calculation with relatively large scale,[9] and the vibronic structure of the state was also studied for both species.[10,11] The excited states of these species were also computationally examined.[12]

SiCN is isovalent with CCN, and the $\tilde{A}\ ^2\Delta$–, $\tilde{B}\ ^2\Sigma^-$–, and $\tilde{C}\ ^2\Sigma^+$–$\tilde{X}\ ^2\Pi$ transitions of CCN were analyzed by Merer and Travis.[13] Since the electronic transition of CNC has also been observed,[14] it is expected to provide information on the isomerization pathway, SiCN ⇌ SiNC, from spectroscopic results.

Since the metal-cyanide and -isocyanide systems have a relatively low isomerization reaction barrier, the system is thought to be one of the suitable systems to study the isomerization mechanism through spectroscopic information. We are therefore continuing some projects on the spectroscopical study of such systems.[15–17] In the present paper, we show our study on silicon containing species, the SiCN/SiNC molecular system, which is taken as one of the targets for our running project. As one of the results of the project, we report here the electronic spectrum of SiCN.

II. EXPERIMENTAL

The experimental setup and computational details have been given in our previous papers.[15–17] Hence, only characteristic parts of the present experiment are briefly mentioned. The SiCN free radicals were generated by the laser ablation technique in a supersonic free jet expansion of Ar. The second harmonic of a pulsed Nd^{3+} YAG laser (Continuum, Surelite II) was used for the ablation power source. The energy of the laser was less than 1 mJ/pulse, and it was tightly focused on the surface of the Si rod using a plano concave lens with focal length of 1 m. Acetonitrile was used as the source of the CN fragments, which are thought to be produced in Ar plasma generated by the laser ablation. The LIF signals were obtained by excitation from the second harmonic output of a pulsed Nd^{3+} YAG laser-pumped dye laser (Quanta-Ray, LAB-170, and Lambda Physik, Scanmate 2E). The resolution of the dye laser was about 0.2 cm^{-1}, and its frequency was calibrated

[a]Author to whom correspondence should be addressed. Electronic mail: fukushim@info.hiroshima-cu.ac.jp

with opto-galvanic lines of Ne for the red fundamental output. The UV fluorescence was detected by a photomultiplier tube (PMT; Hamamatsu, R-928) through a glass filter (Corning, CS 7-59), and the LIF excitation spectrum was measured by scanning the energy of the excitation light source. To achieve higher energy resolution, an étalon could be installed in the laser cavity. The resolution was then improved to about 0.03 cm^{-1}, and the laser frequency was calibrated by reference to the absorption spectrum of I_2 using the fundamental output. For the measurement of the dispersed fluorescence (DF) spectrum, the fluorescence was dispersed through a 0.5 m monochromator (SPEX, 500M). The photo-current signals from the PMT were treated by a gated integrator (Stanford Research, SR-245) after current amplification (Ithaco, 1211). The monochromator was calibrated using Hg lines. The spectral resolution was 20 cm^{-1} (FWHM), and the peak position of the DF could be determined with an estimated accuracy of ±5 cm^{-1}. To measure the strength of the excitation light source scattered into the monochromator, the spectrum was recorded without the ablation laser after the DF spectrum measurements. In all the spectra obtained in the present study, the LIF signal intensities were normalized against the probe laser intensities at each laser shot. The silicon rod (High Purity Chemetals Laboratory, 99.9%), acetonitrile (Katayama Chemical, Special Grade) and the Ar carrier gas (Nippon Sanso, Research Purity) were used without further purification.

Computational works were performed using a workstation (Origin 2000, Silicon Graphics, with eight CPUs of MIPS R10000) in the Information Processing Center of Hiroshima City University.

III. RESULTS

A. Results from calculation

The $\tilde{X}\ ^2\Pi$ state has been studied in some detail by *ab initio* calculations in the SiCN/SiNC system,[9] while the information on the excited states has been scarcely available except for the optimized structures of the $^2\Delta$, $^2\Sigma^+$, and $^2\Sigma^-$ states.[12] Prior to our experiments, *ab initio* calculations for the molecules have been therefore carried out to obtain some information for searching the optical spectrum by utilizing the Gaussian 98 program package.[18] The calculations were carried out under the QCISD level with the 6-311+G(3fd) basis set. These results are listed in Tables I–III for SiCN and SiNC with linear and bent structures. Their energies are schematically shown in Fig. 1, and it also shows the predicted isomerization potential barrier of the ground state.[9] The results for the ground state are consistent with the previous report;[9] i.e., the $^2\Pi$ states are calculated to be the electronic ground states for both SiCN and SiNC having linear geometries in the equilibrium nuclear configurations. Different from our experiences in the AlNC/AlCN and MgNC/MgCN systems, the cyanide, SiCN, is suggested as the lowest energy species. The isocyanide isomer, SiNC, is predicted to lie at about 540 cm^{-1} above SiCN. The vibrational frequencies of the electronic states are calculated numerically. The frequencies for the three vibrational normal modes of the C–N stretching (ν_1), Si–C–N or Si–N–C bending vibrations (ν_2), and Si–CN or Si–NC stretching (ν_3), in the $\tilde{X}\ ^2\Pi$ states are calculated as shown in Tables I–III. The calculated frequencies are quite consistent with those of the previous calculation.[9] The vibrational frequencies of the three normal modes have trends, SiCN > SiNC for the ν_1 and ν_2 modes and SiCN < SiNC for the ν_3 mode. The A' state with bent structure is thought to be metastable on the A' bending surface between the $\tilde{X}\ ^2\Pi$ states of SiCN and SiNC, since the potential minimum, ~4700 cm^{-1}, is lower than the predicted potential barrier on the surface, ~7300 cm^{-1}.[9] We have been able to find no stable state with the A'' symmetry.

In addition to the ground state information, we have obtained predictions on the electronic excited states. The QCISD method can treat only the lowest electronic state among those with a specific symmetry, and thus unfortunately we have not been able to search for the bent A' structures in the excited state. We have obtained three excited states, and the computed results are also listed in Tables I–III. Similar to the $\tilde{X}\ ^2\Pi$ states, the linear geometries are calculated as the conformations without imaginary vibrational frequencies for the excited states. SiCN and SiNC are categorized as 13 electron $C_{\infty v}$ molecules, and the major contribution of the electronic configurations to the ground and excited states is considered as follows:

the ground state

$$[\text{core}](6\sigma)^2(7\sigma)^2(8\sigma)^2\ (2\pi)^4(9\sigma)^2(3\pi)^1 : \tilde{X}\ ^2\Pi$$

the excited state

$$[\text{core}](6\sigma)^2(7\sigma)^2(8\sigma)^2\ (2\pi)^4(9\sigma)^1(3\pi)^2 : \tilde{A}^2\Delta, \tilde{B}^2\Sigma^+, \text{ and } \tilde{C}^2\Sigma^-.$$

According to the state energy in order, we tentatively labelled the excited states as $\tilde{A}$, $\tilde{B}$, and $\tilde{C}$ as shown in Tables I and II. From the analogy with the $\tilde{A}\ ^2\Delta$–$\tilde{X}\ ^2\Pi$ transition of CCN, isovalent with SiCN, the lowest excited states are attributed to the $^2\Delta$ state, which lies about 25 000 and 30 000 cm^{-1} above the $\tilde{X}\ ^2\Pi$ states for SiCN and SiNC, respectively. The $^2\Sigma^+$ states are predicted as the 2nd excited state for both of the isomers. The energies of the 4th and 5th states of SiNC are close, only ~250 cm^{-1} difference, and therefore we attribute the two states to two minima of the same electronic state, $\tilde{C}\ ^2\Sigma^-$. At the numerical vibrational frequency computation only for the two states, we needed to loosen the convergence criterion to one tenth of the usual, and this also supports our interpretation, because this means the potentials around the minima are shallow.

The $^2A''$ bent structure is predicted to lie at about 35 000 cm^{-1} above the $\tilde{X}\ ^2\Pi$ state of SiCN, which lies above all of the states predicted for SiCN and above the $\tilde{A}\ ^2\Delta$ and $\tilde{B}\ ^2\Sigma^+$ states of SiNC, but below the $\tilde{C}\ ^2\Sigma^-$ state of SiNC. There are two possibilities (1) that the $^2A''$ state corresponds to the $\tilde{A}\ ^2\Delta$ or (2) to the $\tilde{C}\ ^2\Sigma^-$ state, but, at the moment, we have not been able to decide which is correct. The reason for the first possibility is natural, i.e., although the $\tilde{C}\ ^2\Sigma^-$ state correlates to A'' symmetry, the $^2\Sigma^-$ state of SiNC lies above the $^2A''$ bent state, and thus it is thought that the $^2A''$ state corresponds to the $\tilde{A}\ ^2\Delta$ state lying below the $^2A''$ state. In this case,

TABLE I. The electronic states predicted from the linear SiCN.[a]

	$\tilde{X}\ ^2\Pi$	$\tilde{A}\ ^2\Delta$	$\tilde{B}\ ^2\Sigma^+$	$\tilde{C}\ ^2\Sigma^-$	[b]
$r_{\mathrm{Si–C}}$	1.857 0	1.797 9	1.788 6	1.783 2	(Å)
$r_{\mathrm{C–N}}$	1.167 7	1.163 1	1.166 9	1.171 6	(Å)
Total energy	−381.640 802	−381.528 312	−381.518 486	−381.492 498	(hartree)
Relative energy[c]	0.0	24 688.71	26 845.31	32 549.10	(cm^{-1})
Total atomic charge[d]					
Si	0.401 346	0.365 531	0.362 352	0.374 614	
C	0.399 011	0.459 695	0.453 605	0.435 377	
N	−0.800 357	−0.825 227	−0.815 957	−0.809 991	
Total atomic spin density[d]					
Si	0.983 133	0.886 563	1.089 874	0.848 271	
C	−0.182 195	0.033 657	−0.444 005	0.197 659	
N	0.199 062	0.079 779	0.354 132	−0.045 929	
Vibrational frequency[e]					(cm^{-1})
ω_1	2151.47	2193.20	2083.94	2104.22	
ω_2	220.76	336.17	350.10	274.39	
	294.89	341.83	350.11	412.86	
ω_3	571.30	648.87	643.54	634.04	

[a]Calculated by the QCISD method with the 6-311+G(3df) basis set.
[b]The symmetries of the states are tentative. See in the text.
[c]Relative energies measured from the $\tilde{X}\ ^2\Pi$ state of SiCN.
[d]Obtained by the SCF method with the 6-311+G(3df) basis set.
[e]The degenerate ω_2 bending modes generate two different vibrational frequencies along the x and y directions.

the isomerization reaction barrier of the $^2A''$ surface would thus be estimated to be higher than this level, i.e.; 10 300 and 5200 cm^{-1} above the bottom of the $^2\Delta$ state of SiCN and SiNC, respectively. There are two reasons for the second possibility: (1) The $^2A''$ state lies above the $\tilde{C}\ ^2\Sigma^-$ state of SiCN, but below that of SiNC, and thus the two minima of the $\tilde{C}\ ^2\Sigma^-$ state of SiNC mentioned above would be related with this situation, $E(\tilde{C}\ ^2\Sigma^-;\ \mathrm{SiCN}) < E(^2A'') < E(\tilde{C}\ ^2\Sigma^-;\ \mathrm{SiNC})$. (2) We can recognize two remarkable points on spin density: (i) the spin density on Si at the $^2A''$ state is relatively small, and

TABLE II. The electronic states predicted from the linear SiNC.[a]

	$\tilde{X}\ ^2\Pi$	$\tilde{A}\ ^2\Delta$	$\tilde{B}\ ^2\Sigma^+$	$\tilde{C}\ ^2\Sigma^-$		[b]
$r_{\mathrm{Si–N}}$	1.741 5	1.723 8	1.699 9	1.713 8	1.748 2	(Å)
$r_{\mathrm{N–C}}$	1.186 8	1.178 2	1.176 7	1.187 9	1.194 3	(Å)
Total energy	−381.638 347	−381.505 137	−381.492 076	−381.464 473	−381.463 327	(hartree)
Relative energy[c]	538.84	29 775.17	32 641.74	38 699.87	38 951.27	(cm^{-1})
[d]	0.0	29 236.33	32 102.90	38 161.03	38 412.43	
Total atomic charge[e]						
Si	0.351 666	0.336 230	0.371 715	0.282 735	0.165 203	
C	0.079 643	0.118 301	0.115 606	0.146 637	0.261 470	
N	−0.431 310	−0.454 530	−0.487 321	−0.429 372	−0.426 674	
Total atomic spin density[e]						
Si	1.005 739	0.925 249	1.014 370	0.813 308	0.348 749	
C	0.151 889	0.134 616	0.135 447	0.136 330	0.645 788	
N	−0.157 628	−0.059 866	−0.149 817	0.050 362	0.005 463	
Vibrational frequency[f]				[g]	[g]	(cm^{-1})
ω_1	2022.57	2152.88	2146.60	2024.25	1825.38	
ω_2	158.68	225.82	265.82	203.64	200.75	
	242.57	250.03	265.90	273.43	290.39	
ω_3	646.08	701.40	750.04	662.20	566.26	

[a]Calculated by the QCISD method with the 6-311+G(3df) basis set.
[b]The symmetries of the states are tentative. See in the text.
[c]Relative energies measured from the $\tilde{X}\ ^2\Pi$ state of SiCN.
[d]Relative energies measured from the $\tilde{X}\ ^2\Pi$ state of SiNC.
[e]Obtained by the SCF method with the 6-311+G(3df) basis set.
[f]The degenerate ω_2 bending modes generate two different vibrational frequencies along the x and y directions.
[g]We needed to loosen the convergence criterion to one tenth of the usual, because of a convergence problem on the numerical computation of the second derivatives for the energy.

TABLE III. The electronic states predicted form the bent SiCN/SiNC.[a]

	A'	A''	
r_{Si-C}	2.048 6	2.005 9	(Å)
r_{Si-N}	1.833 5	1.893 3	(Å)
r_{C-N}	1.217 4	1.207 1	(Å)
∠Si–C–N	62.3	66.9	(deg)
∠Si–N–C	81.7	77.1	(deg)
Total energy	−381.619 309	−381.481 464	(hartree)
Relative energy[b]	4717.23	34 970.71	(cm^{-1})
[c]	4178.39	34 431.87	
Total atomic charge[d]			
Si	0.430 949	0.300 784	
C	0.120 896	0.219 304	
N	−0.551 844	−0.520 088	
Total atomic spin density[d]			
Si	0.789 289	0.583 801	
C	0.166 905	0.345 926	
N	0.043 806	0.070 274	
Vibrational frequency			(cm^{-1})
ω_1	1793.35	2050.17	
ω_2	572.01	625.86	
ω_3	264.03	300.27	

[a]Calculated by the QCISD method with the 6-311+G(3df) basis set.
[b]Relative energies measured from the $\tilde{X}\ ^2\Pi$ state of SiCN.
[c]Relative energies measured from the $\tilde{X}\ ^2\Pi$ state of SiNC.
[d]Obtained by the SCF method with the 6-311+G(3df) basis set.

(ii) that of the one of the $\tilde{C}\ ^2\Sigma^-$ states of SiNC is quite small compared to the other states. To obtain the final decision, more careful calculations would be needed.

B. Results from experiment

After several attempts to search for LIF signals of SiCN/SiNC, the spectrum shown in Fig. 2 was obtained in the near ultraviolet region. A part of this spectrum has

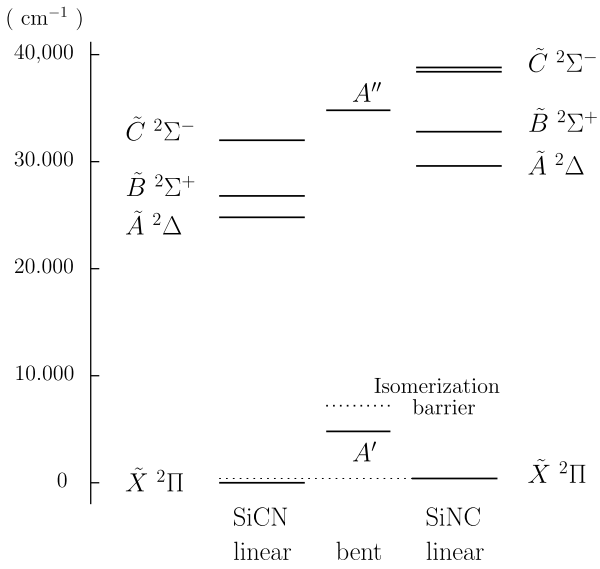

FIG. 1. The electronic states of the SiCN/SiNC system predicted in this work. The predicted isomerization potential barrier is cited from Ref. 9.

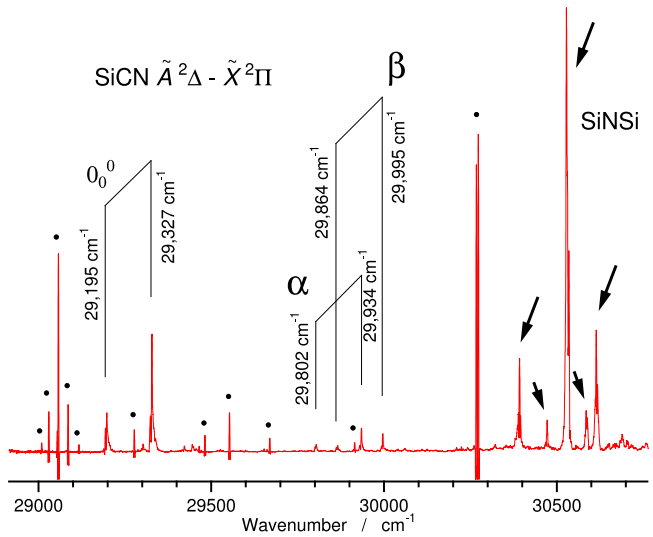

FIG. 2. The LIF excitation spectrum of SiCN observed in the supersonic free jet expansion of Ar. The origins of the electron spin sub-bands are expressed at the side of the vertical lines, such as 29 195 cm^{-1}. Atomic lines of Si are identified in the spectral region, which are pointed out by dots. The five vibronic bands of $\tilde{A}\ ^2\Delta_u$–$\tilde{X}\ ^2\Pi_g$ transition of SiNSi are also observed in this region, which are pointed out by arrows.

been already published in our separate paper on analysis of hot bands of this species.[19] This survey spectrum shows the electronic transitions of Si atoms, which are easily distinguishable from other molecular transitions in view of their spectral line widths and shapes, and short fluorescence lifetimes. Another species detected in this spectrum is the SiNSi radical. The five vibronic bands at ~30 500 cm^{-1} involve two pairs of transitions separated by ~130 cm^{-1} and a single transition. They are assigned as the 0_0^0 transition of the $\tilde{A}\ ^2\Delta_u$–$\tilde{X}\ ^2\Pi_g$ system of SiNSi and the associated weaker hot bands, whose analyses will be reported in the near future.[20] In addition to these species, we can identify another pair of bands with a ~130 cm^{-1} interval, which is close to the SO coupling constant of SiCN/SiNC estimated from the spin densities, ρ_M, under the study (Table I); order of magnitude of A'' is evaluated as $\sum_M \rho_M \zeta_M = 0.983 \times 148.9 + (-0.182) \times 29.0 + 0.199 \times 73.3 = 155.68$ (cm^{-1}), where M shows the elements, Si($3p^2$), C($2p^2$), and N($2p^3$), and the SO constants, ζ_M, are referred to Ref. 31. The survey spectrum actually shows three sets of the bands with this characteristic pattern being assigned as the transitions of the $^2\Delta$–$^2\Pi$ type from their rotational structures. Among them, a pair of the bands at ~29 260 cm^{-1} is the strongest, and they will be attributed to the 0_0^0 band of $\tilde{A}\ ^2\Delta$–$\tilde{X}\ ^2\Pi$ system of SiCN. The following two band systems at ~29 870 and ~29 930 cm^{-1}, labeled α and β, respectively, in order of increasing energies, will be ascribed to the members of the ν_2 and ν_3 progressions, 2_0^2 and 3_0^1, in which the Fermi resonance is remarkable between two $^2\Delta$ vibronic levels. At the higher energy region than the 29 995 cm^{-1} band, we have not observed any vibronic bands attributed to those of SiCN in the LIF excitation spectrum. It is thought that the higher vibronic levels have non-radiative processes, such as (pre-) dissociation, and internal conversion, which can compete with the fluorescence process, and it is

thus expected that they cannot be observed in LIF spectrum, but may be done in absorption.

1. The 0_0^0 band

Figures 3(a) and 4(a) show the rotationally resolved spectra of the two bands lying at 29 327 and 29 195 cm^{-1}, respectively. They consist of P and R branches with a strong Q branch showing a typical structure of a perpendicular transition with non-zero Λ ($\Lambda' \neq 0$ and $\Lambda'' \neq 0$) for linear molecules and provide a clue as to what is the species responsible for the observed spectra. Both of the spectra show the well-separated P branch transitions extending to lower energies and the R branches to higher. It was then easy to assign their P and R transitions using the combination difference $\Delta_2 F''(J)$ for the lower state[21]

$$\begin{aligned}\Delta_2 F''(J) &= R(J-1) - P(J+1) \\ &= 4B''(J+\frac{1}{2}),\end{aligned} \tag{1}$$

where B'' denotes the rotational constant in the lower state. This analysis gives similar B'' constants for the two spectra, $B'' \approx 0.185$ cm^{-1}. The rotational constants thus derived are very close to that of the $\tilde{X}\ ^2\Pi$ ground state of SiCN determined by rotational spectroscopy, 0.1849 cm^{-1}.[4,5] Furthermore, this preliminary analysis indicates that the lowest level identified in the spectrum is $J'' = 1/2$ in the 29 327 cm^{-1} band, and $J'' = 3/2$ in the 29 195 cm^{-1} band. These findings denote that the 29 327 cm^{-1} band is the F_1'–F_1'' transition ($^2\Delta_{\frac{3}{2}}$–$^2\Pi_{\frac{1}{2}}$) of the $\tilde{A}\ ^2\Delta$–$\tilde{X}\ ^2\Pi$ system of SiCN, whose rotational transitions are noted by P_1, Q_1, and R_1 in spectrum (a) of Fig. 3. These also indicate that the 29 195 cm^{-1} band is the corresponding F_2'–F_2'' transition ($^2\Delta_{\frac{5}{2}}$–$^2\Pi_{\frac{3}{2}}$) noted by P_2, Q_2, and R_2 in spectrum (a) of Fig. 4. The occurrence of the $^2\Delta$–$^2\Pi$ transition of SiCN is consistent with the prediction by *ab initio* calculations (Table I). For the isovalent species, CCN, the $\tilde{A}\ ^2\Delta$–$\tilde{X}\ ^2\Pi$ electronic transition has been actually reported.[13]

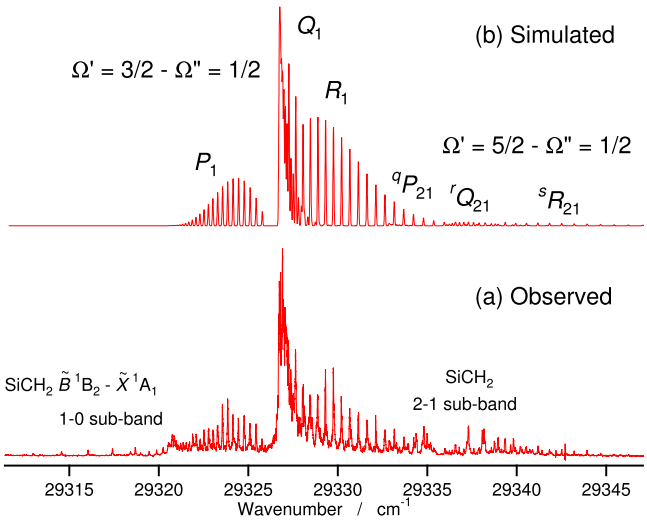

FIG. 3. The rotationally resolved spectrum of the 29 327 cm^{-1} band; the observed (a) and the simulated (b). The rotational temperature of the simulated spectrum is 20 K for the F_1'' component. The $SiCH_2$ $\tilde{B}\ ^1B_2$–$\tilde{X}\ ^1A_1$ transition is also observed in this spectral region.

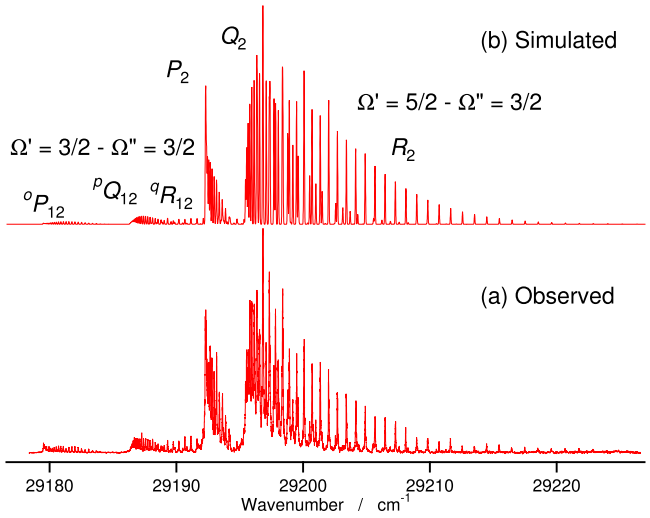

FIG. 4. The rotationally resolved spectrum of the 29 195 cm^{-1} band; the observed (a) and the simulated (b). The rotational temperature of the simulated spectrum is 50 K for the F_2'' component.

In addition to the $\Delta\Sigma = 0$ bands, we are able to identify a series of the transitions with $\Delta\Sigma = \pm 1$ between the different spin components, F_2'–F_1'' and F_1'–F_2''. In spectrum (a) of Fig. 4, the latter transitions, the so-called satellite transitions ($^oP_{12}$, $^pQ_{12}$, and $^qR_{12}$ in the $^2\Delta_{\frac{3}{2}}$–$^2\Pi_{\frac{3}{2}}$ sub-band), are readily seen in the 29 178–29 192 cm^{-1} region. They are by an order of magnitude weaker than the main branches, P_2, Q_2, and R_2, which follow the $\Delta\Sigma = 0$ selection rule under a Hund's case (a) limit. Spectrum (a) of Fig. 3 shows another weak set of satellite transitions, $^2\Delta_{\frac{5}{2}}$–$^2\Pi_{\frac{1}{2}}$, lying in the 29 332–29 350 cm^{-1} region. In this region, there are vibronic bands of the $\tilde{B}^1B_2$–$\tilde{X}^1A_1$ transition of $SiCH_2$,[22,23] and thus the $\frac{5}{2}$–$\frac{1}{2}$ sub-band had initially been unable to analyze due to spectral congestion.

To analyze the vibronic bands consisting of the three sub-bands, the following Hamiltonian has been used:

$$H = H_{\rm rot} + H_{\rm SO}, \tag{2}$$

where $H_{\rm rot}$ and $H_{\rm SO}$ account for the molecular rotation and the SO interaction, respectively. The higher terms, such as Λ-type doubling, were not involved in the analysis, since their parameters were not determined with a reasonable accuracy under our spectral resolution (~0.03 cm^{-1}). To evaluate these matrix elements, we used Hund's case (a) basis functions for both the upper and lower electronic states

$$|v_n; \Lambda, S, \Sigma; J, P, M_J\rangle = |v_{\rm n}\rangle|\Lambda\rangle|S, \Sigma\rangle|J, P, M_J\rangle, \tag{3}$$

where symbols for the quantum numbers are those widely used, and $|v_{\rm n}\rangle$, $|\Lambda\rangle$, $|S, \Sigma\rangle$, and $|J, P, M_J\rangle$ are vibrational, electronic angular momentum, electron spin, and molecular rotation wave-functions, respectively, i.e., the basis functions are a product of the four wavefunctions. The matrix elements on this basis were cited from Refs. 24 and 25. The three sub-bands, i.e., two of the major, $\frac{3}{2}$–$\frac{1}{2}$ and $\frac{5}{2}$–$\frac{3}{2}$, and one of the satellites, $\frac{3}{2}$–$\frac{3}{2}$, were analyzed simultaneously, and the results enabled us to pick up the rotational lines of the $\frac{5}{2}$–$\frac{1}{2}$ satellite sub-band of SiCN in the spectral region with the strong $SiCH_2$ band.

TABLE IV. Molecular constants (cm^{-1}).[a]

Band	This work 0_0^0	This work α	This work β	Ref. 4
$\tilde{A}\ ^2\Delta$				
B'	0.193 249(22)	0.193 429(38)	0.193 515(50)	...
A'	4.944 94(93)	4.926 4(11)	4.929 9(12)	...
ν	29 261.610 3(10)	29 868.424 1(14)	29 930.256 9(15)	
$\tilde{X}\ ^2\Pi$				
B''	0.184 812(22)	0.184 961(38)	0.184 818(51)	0.184 908 3
A''[b]	140.795 1(516)	140.799 7(20)	140.796 7(21)	70.779 9
σ	0.012 03	0.013 34	0.013 08	

[a]Numbers in parentheses are one standard deviation in units of the last significant digit.
[b]The A constants of Si $^3P(3p^2)$ and SiH $\tilde{X}\ ^2\Pi$ are 148.9 and 143.35 cm^{-1}, respectively.

We finally assigned 64 transitions for the $\tilde{A}\ ^2\Delta_{\frac{3}{2}}$–$\tilde{X}\ ^2\Pi_{\frac{1}{2}}$ band, 45 for $^2\Delta_{\frac{5}{2}}$–$^2\Pi_{\frac{1}{2}}$, 82 for $^2\Delta_{\frac{5}{2}}$–$^2\Pi_{\frac{3}{2}}$, and 83 for $\tilde{A}\ ^2\Delta_{\frac{3}{2}}$–$\tilde{X}\ ^2\Pi_{\frac{3}{2}}$. The molecular parameters thus derived are summarized in Table IV. The standard deviation is 0.012 03 cm^{-1}, which is better than the accuracy of measurements anticipated from the laser resolution (0.03 cm^{-1}). Figure 5 summarizes four sub-bands in the $\tilde{A}\ ^2\Delta$–$\tilde{X}\ ^2\Pi$ transition of SiCN analyzed in this study. It should be pointed out that the analyses involving the satellite transitions are important to determine the SO interaction terms both in the $\tilde{A}\ ^2\Delta$ and $\tilde{X}\ ^2\Pi$ states with a reasonable accuracy.

To clarify the characteristics of the upper vibronic level, the single vibronic levels (SVL) DF spectra were measured. Figures 6(a) and 6(b) show the DF spectra of SiCN obtained by the excitation of the 29 327 and 29 195 cm^{-1} bands, respectively. The spectrum (a) has been already published in

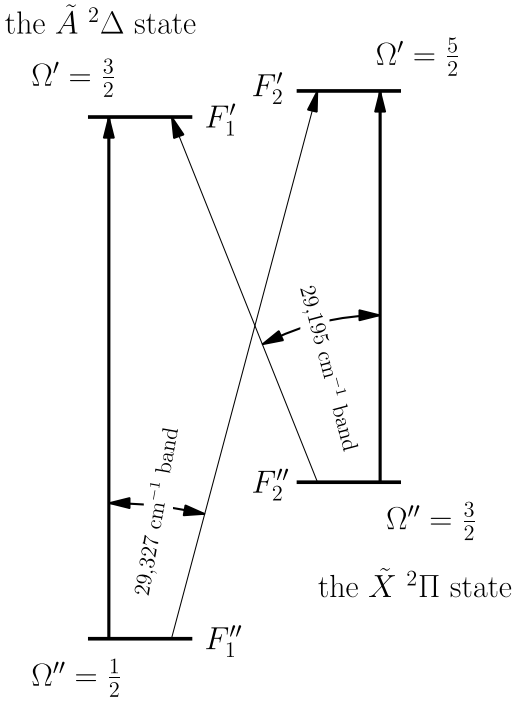

FIG. 5. Schematic diagram of our interpretation of 29 327 and 29 195 cm^{-1} bands. This is the diagram of the $^2\Delta$–$^2\Pi$ electronic transition. Thick arrow indicates stronger intensity than the thin arrow.

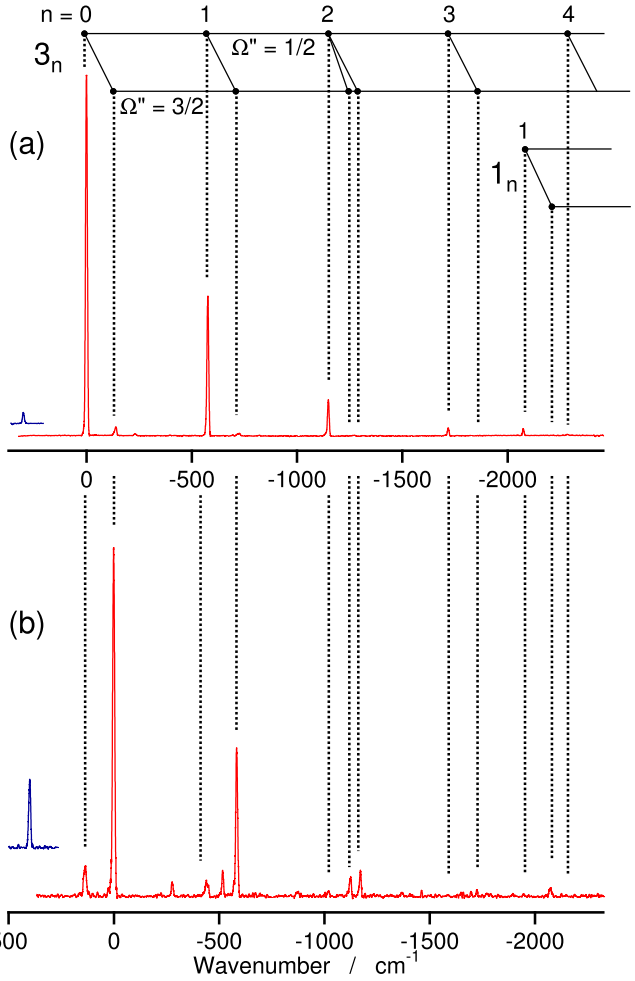

FIG. 6. The LIF DF spectra obtained by the excitation of the 0_0^0 band, $\Omega' = \frac{3}{2}$ (a) and $= \frac{5}{2}$ (b), which are 29 327 and 29 195 cm^{-1} bands in the survey spectrum, Fig. 2, respectively. The spectra are offset by 132 cm^{-1} which is the difference of the excitation energies and which corresponds to the value of the A constant of the $\tilde{X}\ ^2\Pi$ state. The structures which correspond by broken lines then indicate the same terminal vibronic levels. The two vibronic levels, which are terminal levels of two vibronic bands of the third member of 3_2, $\Omega'' = \frac{3}{2}$, are both attributed to be the first over-tone of the ν_3 (Si–CN stretching mode) of the $\Omega'' = \frac{3}{2}$ component (see more details in the text). The horizontal axis of each spectrum represents relative energy from the excitation energy. As a reference for the strength of the excitation light source scattered into the monochromator, the spectra measured at the experimental condition without the ablation laser are inserted. The peak positions and base levels of the stray light signal inserted are shifted, and the actual positions and levels are 0 cm^{-1} and the same with the signal back ground levels, respectively.

our separate paper on analysis of hot bands.[19] The spectrum (a) is obtained by the excitation of the Q_1 band head in the $^2\Delta_{\frac{3}{2}}$–$^2\Pi_{\frac{1}{2}}$ sub-band shown in Fig. 3, and the spectrum (b) by the Q_2 band head in the $^2\Delta_{\frac{5}{2}}$–$^2\Pi_{\frac{3}{2}}$ sub-band shown in Fig. 4. In Fig. 6, we have shifted the spectrum (b) by 132 cm^{-1} to lower energies relative to the spectrum (a) by considering the SO splitting in the $\tilde{A}\ ^2\Delta$ and $\tilde{X}\ ^2\Pi$ states. The bands mapped by using broken lines are then arranged to show that the lower levels are common in these spectra. Both the spectra show a progression with the vibrational interval starting with ~580 cm^{-1}. This interval is in good agreement with the value for the vibrational energy of the ν_3 stretching mode predicted by *ab intio* calculations as listed in

Table I. This progression observed up to $v_3'' = 4$ is reasonably ascribed to that of the ν_3 stretching mode. The two vibronic levels, which are terminal levels of two vibronic bands of the third member of 3_2, $\Omega'' = \frac{3}{2}$, are both identically labeled to be the first over-tone of the ν_3 of the $\Omega'' = \frac{3}{2}$ component, and the reason for the duplicate labels will be explained in our separate paper on analyses of the DF spectra.[26] (In our previous paper on the analysis of hot bands,[19] the duplicate label had not been recognized, but it has been noticed in the analysis of the SVL DF spectra.[26]) The strongest band in this progression is observed at the wavenumber used for the excitation, and the intensity decreases monotonically with an increase of vibrational quantum number of the $\tilde{X}\ ^2\Pi$ state. The two fluorescence spectra shown in Fig. 6 have a band separated by 2074 cm^{-1} from the excitation frequency. This interval is in a good agreement with the vibrational energy of the ν_1 stretching mode predicted by *ab intio* calculations (Table I). The observed bands are weaker by more than one order of magnitude as compared with those in the ν_3 progression. For each spectrum in view of the vibrational interval, they are attributed to the second member of the ν_1 progression, 1_1 (the first member is 0_0, which can be also written as 1_0). Since no band has been detected above the laser frequency in the ν_1 and ν_3 progressions, the band used in the excitation can be assigned as the 0_0^0 band of the $\tilde{A}\ ^2\Delta$–$\tilde{X}\ ^2\Pi$ system. This assignment is consistent with our observation that we could not observe a band ascribed to the $\tilde{A}\ ^2\Delta$–$\tilde{X}\ ^2\Pi$ transition at the energies lower than 29 195 cm^{-1} in the survey spectrum.

The ν_1 and ν_3 progressions are relatively short, and their first member, 0_0 (or it can also be labelled 1_0 or 3_0), is the strongest. It suggests that the equilibrium geometries of SiCN are similar in the $\tilde{A}\ ^2\Delta$ and $\tilde{X}\ ^2\Pi$ states. Our *ab initio* calculations actually predicted that both the Si–CN and C–N bond distances are only slight shortened in the excitation from the $\tilde{X}\ ^2\Pi$ ground state to the $\tilde{A}\ ^2\Delta$ electronic state: 3.4% for Si–CN and 0.4% for C–N.

The spectra shown in Fig. 6 have another two progressions other than the strong progressions arising from the ν_1 and ν_3 stretching modes in the $\tilde{X}\ ^2\Pi$ state. One is the observation of the weak satellite bands separated from the members of the strong ν_1 and ν_3 progressions. For example, spectrum (a) shows the weak band lying at lower frequencies by 141 cm^{-1} away from the 0_0^0 band, while spectrum (b) has the weak band at higher wavenumber. These bands occur due to the splitting of the $\tilde{X}\ ^2\Pi$ state into the $^2\Pi_{\frac{3}{2}}$ and $^2\Pi_{\frac{1}{2}}$ electron spin sub-levels by the SO interaction. Spectrum (a) is observed by following the excitation from the $\tilde{X}\ ^2\Pi_{\frac{1}{2}}$ sub-level to the $\tilde{A}\ ^2\Delta_{\frac{3}{2}}$ sub-level. In addition to the transitions radiating back to the $\tilde{X}\ ^2\Pi_{\frac{1}{2}}$ sub-level, we can expect the additional band terminating on the $\tilde{X}\ ^2\Pi_{\frac{3}{2}}$ sub-level from the $\tilde{A}\ ^2\Delta_{\frac{3}{2}}$ sub-level (see Fig. 5). The $^2\Delta_{\frac{3}{2}}$–$^2\Pi_{\frac{3}{2}}$ sub-band must be weak due to its forbidden character of $\Delta\Sigma \neq 0$ under the Hund's case (a) limit. Since the $^2\Pi_{\frac{3}{2}}$ sub-level lies at the energies higher than the $\tilde{X}\ ^2\Pi_{\frac{1}{2}}$ sub-level, each member of the progressions may consist of the strong $^2\Delta_{\frac{3}{2}}$–$^2\Pi_{\frac{1}{2}}$ sub-band and the associated weak $^2\Delta_{\frac{3}{2}}$–$^2\Pi_{\frac{3}{2}}$ sub-band observed at lower frequencies reflecting the SO splitting of 141 cm^{-1} in the transition in spectra (a). On the other hand, the situation is opposite in spectrum (b), where the $\tilde{A}\ ^2\Delta_{\frac{5}{2}}$ sub-level is prepared in the excitation from the $\tilde{X}\ ^2\Pi_{\frac{3}{2}}$ sub-level. The weak $^2\Delta_{\frac{5}{2}}$–$^2\Pi_{\frac{1}{2}}$ sub-band then lies at higher frequencies relative to the strong $^2\Delta_{\frac{5}{2}}$–$^2\Pi_{\frac{3}{2}}$ sub-band.

TABLE V. Vibrational constants of the $\tilde{X}\ ^2\Pi$ state (cm^{-1}).

$\omega_1{}^0$	2074	C–N stretching[a]
$\omega_2{}^0$	236	Si–C–N bending[b]
$\omega_3{}^0$	580	Si–CN stretching

[a]Fundamental frequency.
[b]Evaluated from the distance between the μ and κ levels of $\tilde{X}\ (02^00)\ ^2\Pi$ using Eqs. (6) and (7). See more details in text.

Another feature of the spectra which should be noticed is some other additional bands. The additional bands are clearly recognized in the spectrum (b), and they are confirmed even in the spectrum (a). The additional bands are attributed to be bands fluorescing to bending vibrational levels. The analysis of the vibrational structure including the additional bands is not straightforward, seems to be due to Herzberg-Teller interaction and Fermi and Sears resonances, as well as Renner-Teller (R-T) interaction, in the $\tilde{X}\ ^2\Pi$ state. This analysis is in progress, and the results will be reported in a separate paper.[26]

Table V summarizes the vibrational constants of the $\tilde{X}\ ^2\Pi$ state. The frequency of the ν_1 stretching mode is the fundamental frequency, and that of the ν_3 mode is evaluated only from the ν_3 progression of the spin sub-level with $\Omega'' = \frac{1}{2}$.

2. The α and β bands ($2_0^2 + 3_0^1$)

Above the 0_0^0 band, there are two vibronic band systems, α and β, with the $^2\Delta$–$^2\Pi$ type rotational structure in the survey spectrum of Fig. 2. Each of them shows four sub-bands with rotational structure similar to those of the 0_0^0 band. As schematically summarized in Fig. 7, the α system consists of the stronger $^2\Delta_{\frac{3}{2}}$–$^2\Pi_{\frac{1}{2}}$ sub-band at 29 934 cm^{-1} with a weak $^2\Delta_{\frac{5}{2}}$–$^2\Pi_{\frac{1}{2}}$ sub-band separated by 10 cm^{-1} to higher frequencies, and the $^2\Delta_{\frac{5}{2}}$–$^2\Pi_{\frac{3}{2}}$ sub-band at 29 802 cm^{-1} with the associated $^2\Delta_{\frac{3}{2}}$–$^2\Pi_{\frac{3}{2}}$ sub-band, originating from the different electron spin sub-level of the $\tilde{X}\ ^2\Pi$ state. The $^2\Delta_{\frac{3}{2}}$–$^2\Pi_{\frac{1}{2}}$ sub-band is stronger by a factor of ~3 than the $^2\Delta_{\frac{5}{2}}$–$^2\Pi_{\frac{3}{2}}$ sub-band at lower frequencies reflecting the cooling of the electron spin sub-levels of SiCN in the $\tilde{X}\ ^2\Pi$ state. The situation in the β band is very similar to that observed in α. The four bands of β lie at higher frequencies by ~61 cm^{-1} away from the corresponding bands in α. Two vibronic transitions are independently analyzed using the same Hamiltonian used for the 0_0^0 band. Table IV lists the molecular constants obtained from 220 and 187 transitions for the α and β bands, respectively. The standard deviation of the fitting is 0.013 34 and 0.013 08 cm^{-1} for α and β, respectively. The interaction between the α and β levels is not apparent in these spectra, and the interactions might be absorbed by the molecular constants effectively even if the interactions exist. The molecular constants for the lower state are consistent with those obtained in the 0_0^0 band, supporting the fact that these transitions originate from the $\tilde{X}\ (00^00)\ ^2\Pi$ level.

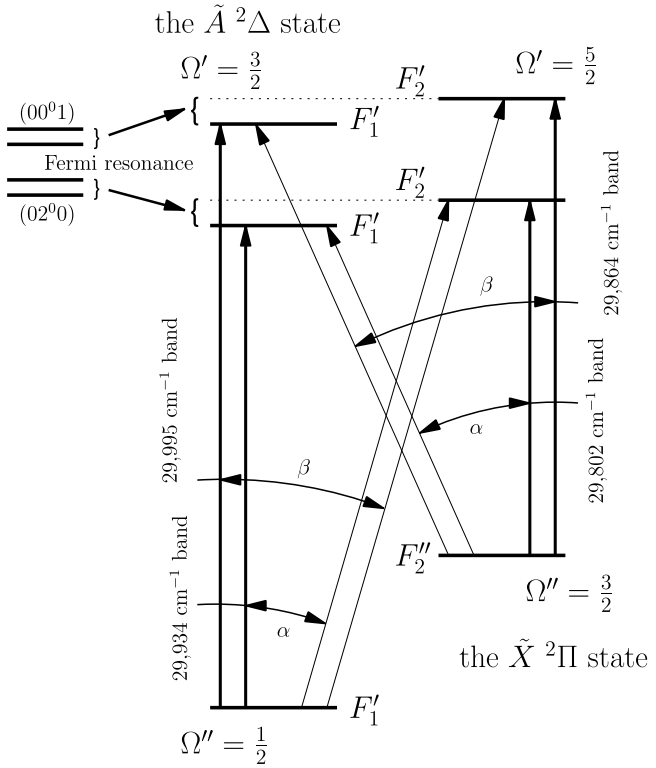

FIG. 7. Schematic diagram of our interpretation of 29 802, 29 864, 29 934, and 29 995 cm^{-1} bands. The upper vibronic levels are affected by Fermi resonance.

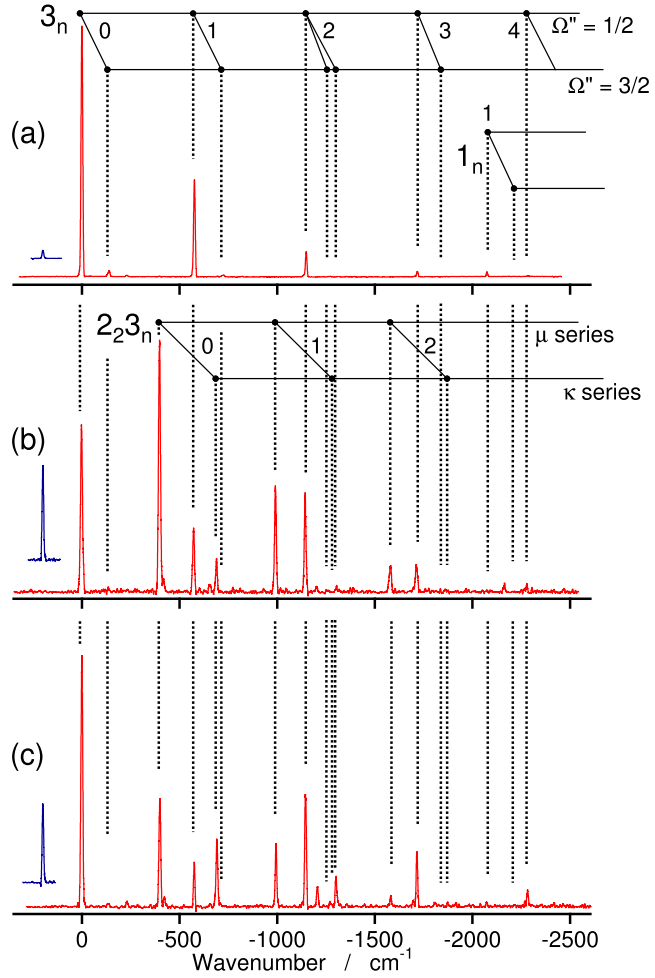

FIG. 8. The LIF DF spectra obtained by the excitation of the $\Omega' = \frac{1}{2}$ spin component of the 0-0, α, and β bands; i.e., the 29 327 (a), 29 934 (b), and 29 995 cm^{-1} bands (c), respectively. The horizontal axis represents the relative energy from the excitation energy. The transitions connected by broken lines then indicate the same terminal vibronic levels. As a reference for the strength of the excitation light source scattered into the monochromator, the spectra measured at the experimental condition without the ablation laser are inserted. The peak positions and base levels of the signal inserted are shifted, and the actual positions and levels are 0 cm^{-1} and the same with the signal background levels, respectively.

To clarify the vibronic character of the upper state, SVL DF spectra were measured for the α and β systems by fixing the laser frequency at the two main bands involved in these transitions. Figures 8(b) and 8(c) show the spectra obtained by the excitation of Q_1 band head of the 29 934 and 29 995 cm^{-1} bands, respectively, where the $\tilde{A}\ ^2\Delta_{\frac{3}{2}}$ vibronic electron spin sub-levels are prepared for the α and β bands, respectively (see Fig. 7). One of the remarkable features of the two spectra (b) and (c) in Fig. 8 is similarity of their vibronic structures. We have also observed the DF spectra from their F_2' components of the $^2\Delta$ states, and this similarity in the F_1' spectra is also recognized in F_2'. This similarity will be the first clue to characterize the fluorescent levels. The spectra (b) and (c) mainly show the vibronic structure of the $\tilde{X}\ ^2\Pi_{\frac{1}{2}}$ sub-level, due to the $\Delta\Sigma = 0$ selection rule under the Hund's case (a) limit, as mentioned in Sec. III B 1. For the spectra (b) and (c), the corresponding transitions to the $\tilde{X}\ ^2\Pi_{\frac{3}{2}}$ sub-levels lying ~141 cm^{-1} away at lower frequencies are expected to be weak and indiscernible but with notable intensity, an observation of which is consistent with that in the spectrum (a) observed from the $\tilde{A}\ (00^00)\ ^2\Delta_{\frac{3}{2}}$ sub-level.

In the three spectra (a)–(c) in Fig. 8, we can easily identify the ν_3 progression with ~580 cm^{-1} interval starting from the band at the excitation frequency. The intensity distributions in the ν_3 progression are similar in spectra (b) and (c), but those intensity features are apparently different from that of spectrum (a) obtained by the 0_0^0 band excitation. In spectra (b) and (c), although the intensity maximum is at the first member, the intensity of the third member is stronger than those of the others; i.e., to the transition terminating on the $\tilde{X}\ (00^02)\ ^2\Pi_{\frac{1}{2}}$ sub-level has a stronger intensity than those on (00^0n), n = 1 and ≥3, and this finding is consistent with the fact that the vibronic level prepared in the $\tilde{A}\ ^2\Delta$ state is vibrationally excited in the ν_3 mode. In terms of the *ab initio* value of $\omega_3' = 649$ cm^{-1} for the $\tilde{A}\ ^2\Delta$ electronic state, we can expect the excitation performed to the $\tilde{A}\ (00^01)\ ^2\Delta_{\frac{3}{2}}$ sub-level in both of the observing spectra (b) and (c). The remarkable difference between the intensity distributions of the ν_3 progression observed from the vibrationless level, $\tilde{A}\ (00^00)\ ^2\Delta$, and those from the α and β vibronic levels are also observed in the spectra of the F_2' component, and will be the second clue to characterize the fluorescent levels.

Besides the ν_3 progression, which is in common in three spectra (a)–(c) in Fig. 8, we can notice the other two ν_3 progressions with their vibrational intervals of ~580 cm^{-1} only in the spectra (b) and (c). The first members of the ν_3 progressions are the bands lying at 399 and 689 cm^{-1} below

the band at the excitation frequency. The progressions are concluded to be $2_2 3_n$ by the following two reasons:

(1) When the ν_2 bending vibration is doubly excited in a Π electronic state, three vibronic species, $\Pi + \Pi + \Phi$, are given. The two $K = 1$ vibronic levels, Π, are then expected to show a large splitting by vibronic interaction, which is known as R-T interaction.[27] The resultant Π vibronic levels are usually denoted by μ Π and κ Π in order of increasing their energies (the lower and higher components are labeled as μ and κ, respectively[28]). Following the R-T model, we have assigned μ and κ series of the progression, $2_2 3_n$, as shown in spectra (b) and (c) in Fig. 8. The Π vibronic levels in the $\tilde{X}\ ^2\Pi$ electronic state can be accessible from $K = 2$ vibronic levels, Δ, of $\tilde{A}\ ^2\Delta$ in fluorescence, which are reached from the $\tilde{X}\ ^2\Pi$ vibrationless level in photo-absorption.

(2) (Understanding of the R-T interaction in computational chemistry) Bending vibration for tri-atomic linear molecules is a doubly degenerate motion and is thought to be a motion in two orthogonal planes including molecular axis. For doublet molecules with $\Lambda \neq 0$, such as the $\tilde{X}\ ^2\Pi$ state of SiCN, the two of the degenerate motion are not equivalent, because one of the plane in motion is along a π molecular orbital (MO) with a lone pair electron and another is orthogonal to the MO. Usually the former has lower frequency than the latter, because the bending vibration of the former has restriction by the π MO, while that of the latter is free for the restriction. The fundamental frequency of the ν_2 modes at the $\tilde{X}\ ^2\Pi$ state of SiCN is predicted to be 220 and 295 cm^{-1} (Table I). Because the frequencies of the first members in the two ν_3 progressions correspond to twice of the fundamentals, they are attributed to the μ and κ components of $2_2 3_n$ with different ω_2'.

The band intensities on the $2_2 3_n$ progression decrease with an increase of the vibrational quantum number, n, of the ν_3 mode in the two series, μ and κ, and the first member, $2_2 3_0$, is the strongest in each progression. These two features on $2_2 3_n$ are similar to the pure 3_n progression in spectrum (a) observed by the $\tilde{A}\ (00^00)\ ^2\Delta_{\frac{3}{2}}$ vibrationless level. The two are also observed in the F_2' spectra, and will be the third clue to characterize the fluorescent levels.

From the three clues mentioned above, it is thus concluded that the upper α and β vibronic levels responsible for spectra (b) and (c) have double faced characters responsible for 3_n and $2_2 3_n$ of the vibrational numbering on the ν_3 mode. In terms of the vibrational frequencies predicted for the ν_2 and ν_3 modes in the $\tilde{A}\ ^2\Delta$ state, 339 and 649 cm^{-1}, respectively, the (02^l0) level is expected to lie closely to the (00^01) level. A single excitation of ν_3 stretching vibration (Σ^+) in a Δ electronic state gives vibronic species, Δ, and a double excitation of ν_2 bending vibration (Π) in a Δ electronic state gives vibronic species, $\Sigma^{(+)} + \Sigma^{(-)} + \Delta + \Gamma$. (In doubly excited bending vibronic level, $v_2 = 2$ and $l = 0$ or ± 2, of "a $^2\Pi$ electronic state," three vibronic levels, $\Pi + \Pi + \Phi$, are generated. The double Π ($K = \pm 1$) vibronic levels are related with $K = \Lambda + l = \pm 1 + (\pm 1 \mp 1)$ and $= \pm 1 + (\mp 1 \mp 1)$ and single Φ ($K = \pm 3$) level corresponds to $K = \pm 1 + (\pm 1 \pm 1)$, where $K = \Lambda + l$ and $l = \sum_{i=1}^{v_2} l_i$, and where K, Λ, l, and l_i are all signed quantum numbers in this statement. Contrastingly, in the level of "a $^2\Delta$ electronic state," four vibronic levels, $\Sigma^{(+)} + \Sigma^{(-)} + \Delta + \Gamma$, are generated. The single Δ ($K = \pm 2$) and Γ ($K = \pm 4$) vibronic levels are related with $K = \pm 2 + (\pm 1 \mp 1)$ and $= \pm 2 + (\pm 1 \pm 1)$, respectively, and two of Σ ($K = 0$) levels consist of $K = \pm 2 + (\mp 1 \mp 1)$.[27] The singly (uniquely) and doubly generated levels, except Σ, are called "unique" and "non-unique" levels, respectively.[29] For the $v_2 = 2$ level of the $^2\Pi$ and $^2\Delta$ electronic states, Φ and $\Delta + \Gamma$, respectively, are the unique level.) In the 29 900 cm^{-1} region, it is therefore reasonable to suppose that two vibronic levels, the $\tilde{A}\ (00^01)\ ^2\Delta$ and unique $(02^00)\ ^2\Delta$ levels, are mixed by Fermi resonance under the condition of $2\omega_2 \approx \omega_3$ in the $\tilde{A}\ ^2\Delta$ electronically excited state, which enables us to interpret the double faced character of the two fluorescent levels.

The Fermi interaction is responsible for the occurrence of strongest $2_2 3_0$ on the $2_2 3_n$ progressions. The Fermi interaction between the $\tilde{A}\ (00^01)$ and $(02^00)\ ^2\Delta_{\frac{3}{2}}$ vibronic levels can prepare two $^2\Delta_{\frac{3}{2}}$ vibronic levels accessible from the $\tilde{X}\ (00^00)\ ^2\Pi_{\frac{1}{2}}$ level. In the ν_2 degenerate bending vibration, the selection rule of $\Delta v_2 = 0, \pm 2, \pm 4, \ldots$ is applied to the vibrational transitions in the $\tilde{A}\ ^2\Delta$–$\tilde{X}\ ^2\Pi$ transition.[27] For the present case, the transition with $\Delta v_2 = 0$ is active, while that with $\Delta v_2 \neq 0$ is inefficient; actually there is no bending ν_2 progression in spectrum (a), the fluorescent level of which is the $\tilde{A}\ (00^00)\ ^2\Delta_{\frac{3}{2}}$ level. The level mixing by Fermi resonance gives the vibronic character of the $\tilde{A}\ (02^00)\ ^2\Delta_{\frac{3}{2}}$ level into the upper two α and $\beta^2\ \Delta_{\frac{3}{2}}$ levels. It indicates that we should find the strong transition to the $\tilde{X}\ ^2\Pi\ v_2'' = 2$ level in the fluorescence spectra from the vibronic level with $v_2' = 2$ vibronic character due to the favorable selection rule of $\Delta v_2 = 0$.

We have also observed the DF spectra from the F_2' components of the $^2\Delta$ states mixed with Fermi resonance by exciting at 29 802 cm^{-1} and 29 864 cm^{-1}. These spectra mainly show the vibronic structure of the $^2\Pi_{\frac{3}{2}}$ sub-level. As same as the F_2' spectrum from the $\tilde{A}\ (00^00)\ ^2\Delta_{\frac{5}{2}}$ vibrationless level, the spectrum (b) in Fig. 6, the F_2' spectra of the α and β levels also have some other additional bands. Their analyses will be reported in a separate paper.[26]

3. Global analysis of the rotational structures

Pure rotational transitions of SiCN were measured with great accuracy in millimeter- and centimeter-wave regions.[4,5] However, the SO constant thus derived is about half of our value, and seems to have a large error because of the lack of the transitions cross combining the $\tilde{X}\ ^2\Pi_{\frac{1}{2}}$ and $^2\Pi_{\frac{3}{2}}$ sub-levels in the analysis by rotational spectroscopy. An analysis was then carried out by combining these data with ours to improve the molecular constants of the $\tilde{X}\ ^2\Pi$ ground state. The data used are 41 pure rotational transitions in the $13.5 \leq J \leq 30.5$ range observed by millimeter-wave absorption spectroscopy. We have not used those (centimeter-wave data) in the $0.5 \leq J \leq 3.5$ range showing the hyperfine structure. The data provided from our observations are 966 of combination differences calculated from the transitions in the three vibronic bands of the $\tilde{A}\ ^2\Delta$–$\tilde{X}\ ^2\Pi$ electronic transition.

We used PGOPHER[30] to fit these data by setting the deviation of measurements with 0.03 cm^{-1} for combination differences and 30 kHz for the pure rotational transitions. The relative weight of the millimeter-wave transition is by a factor of ~30 000 larger than that of the combination difference. The molecular constants of the $\tilde{X}\ ^2\Pi$ ground state thus derived are listed in Table VI, where we used the $\hat{R}$ expression for the Hamiltonian in PGOPHER. The assignments of the observed lines are obtainable from the supplementary material. The SO constant A'' is greatly improved by determining directly from the $^2\Pi_{\frac{3}{2}}$–$^2\Pi_{\frac{1}{2}}$ splitting energy. It leads to give the spin-rotation (SR) constant, γ'', with "negative" value and its higher order term, γ''_D, with reasonable accuracy. The constants derived in the present analysis are consistent with those obtained by the rotational spectroscopy, though it should be pointed out that the SO constant derived in this study is by a factor of 2 larger than that derived by the rotational spectroscopy alone.[4,5] The standard deviation improves from 0.032 MHz to 0.024 42 MHz within their 41 data. The SO constant in the $\tilde{X}\ ^2\Pi$ ground state, $A'' = 140.824\ 14(78)\ cm^{-1}$, is close to that observed in the $^3P(3p^2)$ ground state of Si, 148.9 cm^{-1}.[31] It indicates the unpaired electron is localized mainly on the Si $3p$ orbitals. Such an example is known as the $\tilde{X}\ ^2\Pi$ state of SiH, showing the SO constant of 143.35 cm^{-1}.[32] This result is consistent with that of our *ab initio* calculations (Table I), which indicates the spin density of unpaired electron is mainly localized on the Si atoms and the contribution of Si $3p$ orbital is dominant in the 3π orbitals occupied by an unpaired electron. A computational work on the $\tilde{X}\ ^2\Pi$ state of the SiCN/SiNC system resulted in spin splitting between the vibrationless level of the $\tilde{X}\ ^2\Pi$ state with almost the same with our results.[11]

It is thought from the constants in Table VI that the reason for the halving of the SO constant by rotational spectroscopy[4,5] may be their assumption of "positive" γ''.

Based on the molecular constants thus obtained for the $\tilde{X}\ ^2\Pi$ ground state, three vibronic bands were re-analyzed simultaneously. The molecular constants, obtained for the three vibronic levels by fixing the constants for the $\tilde{X}\ ^2\Pi$ state, are listed in Table VI, where we used the $\hat{R}$ expression for the Hamiltonian in PGOPHER. The assignments of the observed lines are obtainable from the supplementary material. The molecular constants are quite similar in the three vibronic states observed in the $\tilde{A}\ ^2\Delta$ electronically excited state. The vibrational dependence of the constants has been discussed in our previous paper,[19] combining with those obtained from the hot band analyses. The five vibronic levels of the $\tilde{A}\ ^2\Delta$ state, which we have analyzed in the present work and in our previous study,[19] are all unique level, and therefore no information of the R-T interaction on the $\tilde{A}\ ^2\Delta$ state has been obtained unfortunately. The SO constant of the $\tilde{A}\ ^2\Delta$ state is more than by an order of magnitude smaller than that observed in the $\tilde{X}\ ^2\Pi$ ground state. The $\tilde{A}\ ^2\Delta$ excited state has an unpaired electron in 9σ orbital, and the major contribution to the orbital seems to be $3s$ of Si from our *ab initio* calculation and from the previous report.[9] Under the conditions, the SO interaction is expected to be very weak in the $\tilde{A}\ ^2\Delta$ state as observed in the present experiment. The α and β bands lying at frequencies higher than the 0_0^0 band are attributed to the transitions terminating on the $\tilde{A}\ (02^00)\ ^2\Delta$ and $(00^01)\ ^2\Delta$ levels coupled with Fermi resonance. Fermi interaction is known to cause a shift of the vibrational levels from their unperturbed positions, and also to change the

TABLE VI. Molecular constants (cm^{-1}).[a]

Band	0_0^0	α	β			
	This work				Ref. 4	
	$\tilde{A}\ ^2\Delta$[b]					
B'	0.193 322 1(18)	0.193 272 9(28)	0.193 596 0(41)		...	
A'	4.944 83(70)	4.926 33(77)	4.928 85(84)		...	
$K'A'$[c]	9.889 66	9.852 66	9.857 70			
ν	29 261.639 89(81)	29 868.464 69(98)	29 930.285 0(11)		...	
σ	0.013 74	←	←			
	$\tilde{X}\ ^2\Pi$[d]			[e,f]	[f]	
B''	0.184 908 47(26)	←	←	5 543.430 77(77)	5 543.4152(2)	
A''[g]	140.824 14(78)	←	←	422 180 2(23)	212 400 0(6000)	$A''+\gamma''$
γ''	−0.054 301(13)	←	←	−1627.89(40)	2070(10)	
p''	$7.754(27)\times10^{-4}$	←	←	23.245(81)	25.734(2)	$p''+2q''$
q''	$4.136(15)\times10^{-5}$	←	←	1.240 0(45)	0.869(2)	
D''	$7.702\,9(17)\times10^{-5}$	←	←	$2.309\,26(52)\times10^{-3}$	$2.3102(2)\times10^{-3}$	
p''_D	$-1.28(14)\times10^{-8}$	←	←	$-3.82(42)\times10^{-4}$	$-3.86(7)\times10^{-4}$	$(p''+2q'')_D$
γ''_D	$5.81(11)\times10^{-7}$	←	←	0.017 41(34)	Not included	
σ	0.023 47			0.024 42[h]	0.032	

[a]Numbers in parentheses are one standard deviation in units of the last significant digit.
[b]The $\hat{R}$ expression for the Hamiltonian is used for the setting of PGOPHER.
[c]This is a product of the A' constant with quantum number, K', and is just twice of A' in the present case.
[d]The results from combined analysis of the present combination difference data and the microwave data.[4]
[e]The combined analysis in MHz units.
[f]In MHz.
[g]The A constants of Si $^3P(3p^2)$ and SiH $\tilde{X}\ ^2\Pi$ are 148.9 and 143.35 cm^{-1}, respectively.
[h]σ within 41 mm-wave lines.

effective B values of two interacting states. The vibronic level dependence of the effective B values is expressed as follows:[21]

$$B_{[v_i]} = B_e - \sum_{i=1}^{3} \alpha_i (v_i + \frac{d_i}{2}) + \gamma_{22} l^2, \tag{4}$$

where d_i is the degree of degeneracy of the vibrational mode i, and the subscript $[v_i]$ stands for all the vibrational quantum numbers. The B_e value is the rotational constant in the equilibrium geometry. The constants α_i are expected to be positive for the ν_1 and ν_3 stretching modes, while it is negative for the ν_2 bending mode in SiCN. Actually, we observed that the rotational constant in the α level decreases as compared with that in the $\tilde{A}$ (00^00) $^2\Delta$ level, and that in the β level increases. The results might suggest that the $\tilde{A}$ (00^01) $^2\Delta$ level lies at energies lower than the $\tilde{A}$ (02^00) $^2\Delta$ level. It is consistent with the observation that the α band is slightly stronger than the β band, because it is expected from the DF spectrum from the $\tilde{A}$ (00^00) $^2\Delta$ level (Fig. 6(a)) that the transition to the $\tilde{A}$ (00^01) $^2\Delta$ level from $\tilde{X}$ (00^00) $^2\Pi$ is more favorable than that to $\tilde{A}$ (02^00) $^2\Delta$. Further analysis regarding these two interacting states is not possible at the present stage, since the Fermi interaction is absorbed into the rotational constants effectively.

IV. DISCUSSION

A. Bending frequency, ω_2, and the R-T parameter, ϵ, of the $\tilde{X}$ $^2\Pi$ state

The R-T parameter, ϵ, is defined as

$$\epsilon = \frac{V^+ - V^-}{V^+ + V^-} = \frac{(\omega^+)^2 - (\omega^-)^2}{(\omega^+)^2 + (\omega^-)^2}, \tag{5}$$

where ω^+ and ω^- are the bending frequencies for the harmonic potentials, V^+ and V^-, respectively.[27] The ϵ parameter can be evaluated from the energy separation, $2r$ $(=E_\kappa - E_\mu,\ E_\kappa > E_\mu)$, between the μ and κ levels of the $\tilde{X}$ (02^00) $^2\Pi$ vibronic level.[28,33] $2r$ has the following relation with the SO constant, A, and the bending vibrational frequency, ω_2, of the electronic state (see Fig. 8 of Ref. 17)

$$\begin{aligned}(2r)^2 &= (E_\kappa - E_\mu)^2 \\ &= {A_{\text{eff}}}^2 + \left\{\omega_2 \epsilon \sqrt{(v_2+1)^2 - K^2}\right\}^2.\end{aligned} \tag{6}$$

The bending vibronic structure of a $\tilde{X}$ $^2\Pi$ electronic state does not follow the usual expression, such as $E_{v_2} = \omega_2(v_2+1) + x_{22}(v_2+1)^2$.[27] Under a model under a perturbation approach for R-T interaction of a $^2\Pi$ electronic state,[28,33] the energies of the $\tilde{X}$ (02^00) μ and κ $^2\Pi$ bending vibronic levels, E_μ and E_κ, respectively, have the following relation (see Fig. 8 of Ref. 17):

$$\begin{aligned}\frac{1}{2}(E_\mu + E_\kappa) &= 2\,\omega_2 + C_{(02^00)} - C'_{(00^00)} + \frac{1}{2}(A - 2B), \\ C &= -\frac{1}{8}(v_2+1)\epsilon^2\omega_2, \\ C' &= -\frac{1}{8}(v_2+1)(v_2+2)\epsilon^2\omega_2,\end{aligned} \tag{7}$$

where B and A are the rotational and SO constants, respectively, and C and C' correspond to parameters for non-unique and unique vibronic levels, respectively.

Adopting E_μ and E_κ, 399 and 689 cm^{-1}, respectively,[26] and using Eqs. (6) and (7), we can obtain the following simultaneous equations:

$$\begin{cases} (689 - 399)^2 = 138^2 + 8\epsilon^2\omega_2^2 & \text{from Eq. (6)}, \\ \frac{1}{2}(689 + 399) = 2\,\omega_2 - \frac{1}{8}\epsilon^2\omega_2 + 69 & \text{from Eq. (7)}. \end{cases}$$

From the equations, ω_2 is evaluated to be 236 cm^{-1}, as listed in Table V. The ϵ parameter is evaluated to be 0.38.

B. Temperature

We have simulated the rotationally resolved spectra to establish the experimental conditions in taking the spectra. For this purpose, Hönl-London factors for the Δ–Π electronic transition under the intermediate case between Hund's case (a) and (b) were referred from the literature.[34] The spectra were simulated from 10 K to 90 K with an interval of 10 K using the molecular constants listed in Table IV. The observed spectra always showed non-Boltzmann distribution in the lower electronic state, $\tilde{X}$ $^2\Pi$, and the rotational temperature could be estimated with the accuracy of ±5 K. To determine the rotational temperature, the rotational structure of the observed spectrum was compared with those simulated, and the best fitted one was selected. The ±5 K accuracy was thus achieved.

Figure 3(b) shows the results for the spectrum observed from the lower spin sub-level, $^2\Pi_{\frac{1}{2}}$, in the 0_0^0 band, which can reproduce spectrum (a) with the rotational temperature of 20 K. In the 0_0^0 band, we failed to reproduce the features of the spectrum from the upper spin sub-level, $^2\Pi_{\frac{3}{2}}$, with the same temperature, but could do with the temperature of 50 K, as shown in Fig. 4(b). The spectral intensity ratio between the transitions from the $^2\Pi_{\frac{3}{2}}$ and $^2\Pi_{\frac{1}{2}}$ levels is derived to be roughly 1:3 from the band intensities observed at 29 195 and 29 327 cm^{-1}. The temperature for describing the distribution in two spin sub-levels is then estimated to be about 180 K, using the SO constant in the $\tilde{X}$ $^2\Pi$ ground state. We have also observed vibrationally hot bands on the ν_2 fundamental,[19] and the vibrational temperature of the $\tilde{X}$ $(01^10)^2\Delta$ level was estimated to be 130 K using ~7% intensity of the hot $^2\Phi$–$^2\Delta$ band by comparing with the cold $^2\Delta$–$^2\Pi$ band and using $\omega_2 = 236$ cm^{-1}. The rotational temperatures of the lower vibrational levels of the hot bands, (01^10) μ $^2\Sigma^{(-)}$, $^2\Delta_{\frac{1}{2}}$, and $^2\Delta_{\frac{3}{2}}$, were estimated to be 30 K using the same procedure described above, though the temperatures have relatively large uncertainties due to the relatively low LIF intensities.

Rotational, vibrational, and electron spin temperatures of jet cooled species at the observed region, i.e., at collision free region in supersonic free jet expansion, are achieved through energy transfer between translational mode of carrier gas and three modes of the species, the rotational, vibrational, and electron spin modes, respectively, at the expansion region, i.e., through rotationally, vibrationally, and electron spin collisional relaxations, respectively, with carrier gas. The efficiencies of the collisional relaxations are considered

through three points of view: (1) level spacings of the modes, (2) energy gaps among stacks of the level, and (3) selection rules among the stacks. In the view of "level spacings" of the first item (1), the efficiency of collisional relaxation, i.e., collisional energy transfer from the three modes to translation of rare gases, can be discussed as follows: it is suggested that the collisional relaxation on systems with level spacing energy close to the collision energy is more efficient than that with one far from the energy, due to a sort of resonance effect. Because the collision energy is closer to the level spacing energy of the rotational structure than that of the vibrational, it is actually suggested that R-T (rotational-translational) transfer is more efficient than V-T (vibrational-translational) transfer.[35] The first item, level spacings, also suggests that energy transfer between systems with similar level spacing energy is more efficient due also to the resonance effect, e.g., V-V (vibrational-vibrational) and R-R (rotational-rotational) energy transfers are more efficient than V-R.[35] The relatively low temperatures observed for the rotational mode among the others, vibrational and electron spin modes, are thus understandable.

The second item (2) suggests that energy transfer (i.e., transition) among stacks of levels in systems with smaller energy gaps among the stacks is more efficient than those with larger gaps. For example, as shown in Fig. 9(a), when energy gaps between vibrational stacks are small, many rotational levels have proximity to those with similar J in the other stacks, and the energy transfer becomes efficient due to the resonance effect discussed above at the first item. Contrary, when the energy gaps are large, it is merely expected that a few rotational levels accidentally have proximity to those with distant J in the other stacks, and then the transitions among the stacks are in-efficient. On the present SiCN system with the condition, $2B$ (=0.37 cm^{-1}) $\ll$ ω_2 (=236 cm^{-1}), the relatively high vibrational temperature, which enables us to observe the vibrationally hot bands,[19] is understandable.

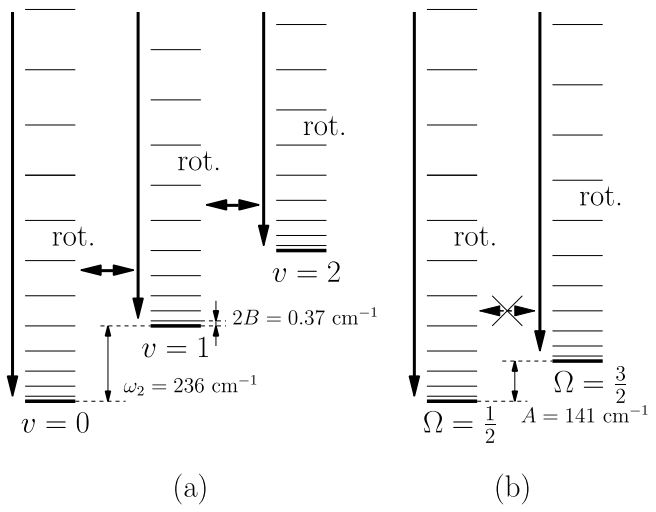

FIG. 9. The level diagram of the vibrational (a) and spin (b) levels, and collisional cooling processes in the level structures. Collisional transition between vibrational levels is allowed, while that between the spin sub-levels is forbidden. "rot." means rotational structure. The down arrows indicate collisional relaxation in a rotational structure.

As suggested by the last item (3), there is a selection rule in the collisional relaxations. The collisional relaxations by rare gas do not have any effect upon electron spin under lower order approximation of theory, and thus the collisional transition between electron spin sub-levels is forbidden. The highest temperature of the electron spin mode is also understandable, even though smaller energy gap between the spin-sub-levels, A = 140 cm^{-1}, than that of the vibrational mode, ω_2 = 236 cm^{-1}.

It is expected that rotational structures of the two electron spin sub-levels, $^2\Pi_{\frac{3}{2}}$ and $^2\Pi_{\frac{1}{2}}$, are almost the same, because B's for the sub-levels are almost the same. It is thus considered that R-T collisional relaxation in stacks of each electron spin component would not be so different. It is thus expected that the similar rotational temperature in the two sub-levels, because of the similarity of the rotational structure of the two spin components, and because of the isolate situation of each stack due to the forbidden transition between the spin-components. At present, we cannot thus give any reasonable explanation to the present observation of the different rotational temperatures, 20 and 50 K, for the two spin sub-levels, $\tilde{X}\ ^2\Pi_{\frac{1}{2}}$ and $^2\Pi_{\frac{3}{2}}$, respectively. The difference of the depth for the cooling process, ~140 cm^{-1}, i.e., the difference of the energy gap between the two spin sub-levels may reflect the temperature difference. The extra length, ~140 cm^{-1}, for the collisional cooling process of the $\tilde{X}\ ^2\Pi_{\frac{1}{2}}$ level may be effective for the extra cooling of the level. The rotational temperatures, 30 K, of the three vibrational levels, (01^10) $\mu\ ^2\Sigma^{(-)}$, $^2\Delta_{\frac{1}{2}}$, and $^2\Delta_{\frac{3}{2}}$, are lower than that of the lower level, 50 K at (00^00) $^2\Pi_{\frac{3}{2}}$, though the former three have relatively large uncertainties. The situation of the $^2\Delta$ unique level is almost the same with that of the (00^00) $^2\Pi$ unique level, but the former has the level, $\mu\ ^2\Sigma^{(-)}$, just ~30 cm^{-1} below the $^2\Delta_{\frac{1}{2}}$, as an additional level (see Fig. 8 in Ref. 19). Because (01^10) $\mu\ ^2\Sigma^{(-)}$ has both of $\Omega = \frac{1}{2}$ and $= \frac{3}{2}$ characters,[27,28] the collisional relaxation between the (01^10) $^2\Sigma^{(-)}$ and the $^2\Delta$ unique level, both $^2\Delta_{\frac{1}{2}}$ and $^2\Delta_{\frac{3}{2}}$ levels, is possible. The inverse temperature observed is thought to be caused by advantageous collisional relaxation among the three vibrational levels, due to the relatively closely lying situation of the three.

SUPPLEMENTARY MATERIAL

See supplementary material for the simultaneous analysis of the combination differences derived from the present LIF data with the previously reported rotational transitions and the assignments of the observed lines on the present study.

ACKNOWLEDGMENTS

The authors are thankful to Yoshihiro Sumiyoshi and Michael C. McCarthy for their useful discussion, and to correspondence from Jesúe R. Flores and Aldo J. Apponi. The authors are also thankful to Colin M. Western for useful suggestions on usage of PGOPHER. The computational resources at the Information Processing Center of Hiroshima City University are acknowledged for executing

the computational part of the present work. This research was supported in part by the Ministry of Education, Science, Sports and Culture, Grant-in-Aid for Scientific Research©, No. 16510078, 2004, and by Hiroshima City University Grant for Special Academic Research (General Studies), No. 4105.

[1]I. P. Herman, Chem. Rev. **89**, 1323 (1989).
[2]E. Kagi and K. Kawaguchi, J. Mol. Spectrosc. **199**, 309 (2000).
[3]G. Maier, H. P. Reisenauer, H. Egenolf, and J. Glatthaar, Eur. J. Org. Chem. **1297**, 1307 (1998), http://onlinelibrary.wiley.com/doi/10.1002/(SICI)1099-0690(199807)1998:7%3C1307::AID-EJOC1307%3E3.0.CO;2-Z/full.
[4]A. J. Apponi, M. C. McCarthy, C. A. Gottlieb, and P. Thaddeus, Astrophys. J. **536**, L55 (2000).
[5]M. C. McCarthy, A. J. Apponi, C. A. Gottlieb, and P. Thaddeus, J. Chem. Phys. **115**, 870 (2001).
[6]A. Largo-Cabrerzio and J. R. Flores, Chem. Phys. Lett. **147**, 90 (1988).
[7]A. Largo-Cabrerzio, Chem. Phys. Lett. **147**, 95 (1988).
[8]M. Guélin, S. Muller, J. Cernicharo, A. J. Apponi, M. C. McCarthy, C. A. Gottlieb, and P. Thaddeus, Astron. Astrophys. **363**, L9 (2000), http://aa.springer.de/papers/0363001/2300l9/small.htm.
[9]N. A. Richardson, Y. Yamaguchi, and H. F. Schaefer III, J. Chem. Phys. **119**, 12946 (2003).
[10]I. Tokue and S. Nanbu, Chem. Phys. Lett. **514**, 239 (2011).
[11]V. Brites, A. O. Mitrushchenkov, and C. Léonard, J. Chem. Phys. **138**, 104311 (2013), there is a questionable point on this paper. The spin-orbit constant of SiCN of the $\tilde{X}\ ^2\Pi$ state is reported to be 73.8 and 70.5 cm^{-1} for the r_e and r_0 structure, respectively, while the spin splitting at the vibrationless levels, $\tilde{X}\ (00^00)\ ^2\Pi_{1/2}$ and $^2\Pi_{3/2}$, is reported to be 141 cm^{-1}. Because the spin splitting, ΔE, can be approximated with $\Delta E = A\Lambda - 2B$,[25] there is inconsistency between their A and ΔE.
[12]J. R. Flores, Chem. Phys. **310**, 303 (2005).
[13]A. J. Merer and D. N. Travis, Can. J. Phys. **43**, 1795 (1965).
[14]A. J. Merer and D. N. Travis, Can. J. Phys. **44**, 353 (1966).
[15]M. Fukushima and T. Ishiwata, J. Mol. Spectrosc. **216**, 159 (2002).
[16]M. Fukushima and T. Ishiwata, J. Mol. Spectrosc. **233**, 210 (2005).
[17]M. Fukushima and T. Ishiwata, J. Chem. Phys. **127**, 044314 (2007).
[18]M. J. Frisch, G. W. Trucks, H. B. Schlegel, G. E. Scuseria, M. A. Robb, J. R. Cheeseman, V. G. Zakrzewski, J. A. Montgomery, Jr., R. E. Stratmann, J. C. Burant, S. Dapprich, J. M. Millam, A. D. Daniels, K. N. Kudin, M. C. Strain, O. Farkas, J. Tomasi, V. Barone, M. Cossi, R. Cammi, B. Mennucci, C. Pomelli, C. Adamo, S. Clifford, J. Ochterski, G. A. Petersson, P. Y. Ayala, Q. Cui, K. Morokuma, D. K. Malick, A. D. Rabuck, K. Raghavachari, J. B. Foresman, J. Cioslowski, J. V. Ortiz, A. G. Baboul, B. B. Stefanov, G. Liu, A. Liashenko, P. Piskorz, P. Komaromi, R. Gomperts, R. L. Martin, D. J. Fox, T. Keith, M. A. Al-Laham, C. Y. Peng, A. Nanayakkara, C. Gonzalez, M. Challacombe, P. M. W. Gill, B. Johnson, W. Chen, M. W. Wong, J. L. Andres, C. Gonzalez, M. Head-Gordon, E. S. Replogle, and J. A. Pople, GAUSSIAN 98, Revision A.9, Gaussian, Inc., Pittsburgh, PA, 1998.
[19]M. Fukushima and T. Ishiwata, J. Phys. Chem. A **117**, 9435 (2013).
[20]M. Fukushima, T. Ishiwata, C. Motoyoshi, Y. Sumiyoshi, and Y. Endo, "Laser induced fluorescence spectroscopy of the SiNSi radical" (to be published).
[21]G. Herzberg, *Spectra of Diatomic Molecules*, 2nd ed. (Van Nostrand Company, Inc., Princeton, NJ, 1950).
[22]H. Leclercq and I. Dubois, J. Mol. Spectrosc. **76**, 39 (1979).
[23]W. W. Harper, K. W. Waddell, and D. J. Clothier, J. Chem. Phys. **107**, 8829 (1997).
[24]R. N. Zare, *Angular Momentum* (John Wiley & Sons, Inc., New York, NY, 1988).
[25]H. W. Kroto, *Molecular Rotation Spectra* (John Wiley & Sons Ltd., London, 1975).
[26]M. Fukushima and T. Ishiwata, "Dispersed fluorescence spectroscopy of the SiCN $\tilde{A}\ ^2\Delta - \tilde{X}\ ^2\Pi$ system," J. Chem. Phys. (to be published).
[27]G. Herzberg, *Electronic Spectra of Polyatomic Molecules* (Van Nostrand Company, Inc., Princeton, NJ, 1950).
[28]J. T. Hougen, J. Chem. Phys. **36**, 517 (1962).
[29]Ch. Jungen and A. J. Merer, "The Renner-Teller effect," in *Molecular Spectroscopy: Modern Research Vol. II*, edited by K. N. Rao (Academic Press, New York, 1976).
[30]PGOPHER, a Program for Simulating Rotational Structure, C. M. Western, University of Bristol, 2010, http://pgopher.chm.bris.ac.uk.
[31]H. Léfèbvre-Brion and R. W. Field, *Perturbations in the Spectra of Diatomic Molecules* (Academic Press, Inc., Orlando, FL, 1986).
[32]A. E. Douglas, Can. J. Phys. **35**, 71 (1956).
[33]J. M. Brown and F. Jorgensen, Adv. Chem. Phys. **52**, 117 (1983), http://onlinelibrary.wiley.com/doi/10.1002/9780470142769.ch2/summary.
[34]I. Kovacs, *Rotational Structure in the Spectra of Diatomic Molecules (Translated by L. Nemes)* (Adam Hilger Ltd., London, NW, 1969).
[35]R. D. Levine and R. B. Bernstein, *Molecular Reaction Dynamics and Chemical Reactivity* (Oxford University Press, New York, NY, 1987).